Sensory Fusion of Magnetoinertial Data Based on Kinematic Model With Jacobian Weighted-Left-Pseudoinverse and Kalman-Adaptive Gains

Matjaž Mihelj, *Member, IEEE*, Janez Podobnik, and Marko Munih, *Member, IEEE*

Abstract—This paper presents a sensory fusion method for estimation of joint angles of serial kinematic chains with rotational degrees of freedom based on magnetoinertial measurements—Magnetoinertial tracking based on JAcobian PseudoInverse (MIJAPI). The concept takes into account the mechanism kinematic model, and the computation relies on the differential kinematics inversion (inverse kinematics solution based on the Jacobian inverse). A Moore–Penrose weighted left pseudoinverse of the mechanism Jacobian matrix is applied to solve a (typically) overdetermined system (redundant measurements resulting from constraints related to attachments of magnetoinertial sensors) in a least-squares approach. Calculation of a gain matrix for correcting the estimated angles is based on Kalman-adaptive algorithm. The quality of the proposed approach was compared to different solutions based on the Unscented Kalman filter. In terms of computational complexity, the MIJAPI concept outperforms the Kalman-based approaches. Better results were also noticed in conditions with significant measurement disturbances and sensor misalignments. The method is applicable in the fields of human motion tracking/analysis as well as robotics.

Index Terms—Human–computer interaction, Kalman filter, kinematics, motion analysis, motion artifacts, motion estimation, sensor fusion.

I. INTRODUCTION

MOTION tracking and movement analysis are the applications that typically deal with serial kinematic chains with the goal of measuring (estimating) joint angles. Magnetoinertial measurement units (IMUs) are commonly used in various applications for motion tracking [1]. In this paper, we focus on serial kinematic chains with rotational degrees of freedom (DoFs), such as a human body or a serial robot that is equipped with IMUs. Human motion tracking is being used in rehabilitation in general, and it is also important in robot-aided rehabilitation [2]. While in cases where robotic devices are exoskeletons, user joint angles can be deduced from robot joint angles, many simpler robotic devices are endpoint devices, which require additional motion tracking system to measure the user joint angles, either for control or assessment. Motion tracking is also finding use in collaborative robotics. Control of collaborative robots should include safety strategies that would guarantee human safety. Researchers have proposed precollision safety strategies that are based on motion tracking of the body and limb movements of the worker to determine restricted space, in which the robot cannot enter [3].

Typical solutions for sensory fusion of magnetoinertial data is Kalman filter in one of its (nonlinear) formulations, such as extended [4] or unscented Kalman filter [5]. A computationally more efficient solution is obtained in the form of a (nonlinear) complementary filter [6]. In order to reduce the dimension of the state vector and make the measurement equations linear, the acceleration and magnetometer measurements can be preprocessed using the Quest algorithm, resulting in a quaternion input for the filter [7]. Martin and Salaün [8] developed invariant extended Kalman filter that takes into account geometrical properties of equations for quaternion-based orientation estimation of a single IMU for aerospace applications. Invariant extended Kalman filter is variant of the extended Kalman filter with advantages of invariant filter, which takes into account natural invariances of the nonlinear operations (e.g., rotation) [9]. In general, extended Kalman filter does not preserve the invariances, whereas invariant extended Kalman filter does preserve them [8], and as a consequence, in invariant extended Kalman filter, the Kalman gain matrix and covariance matrices converge to constant values. This results in a faster convergence of the estimation and a larger expected domain of convergence. A review of sensor fusion and filtering techniques proposed for inertial/magnetic orientation tracking can be found in [1].

Most of the filters are designed for estimation of orientation based on outputs of a single IMU and do not take into account kinematic constraints imposed by the joints of the mechanism [10]. However, there are solutions that require kinematic model for precise motion tracking. An algorithm for estimating linear accelerations during walking and running motions, thus improving the accuracy of inertial motion capture, is presented in [11]. Seel *et al.* [12], [13] exploit the kinematic constraints introduced by hinge and spheroidal

joints for joint axis and position estimation. A method that fuses the measured segment's angular velocity and linear acceleration via known kinematic relations between segments is proposed in [14]. In [15], a method that uses Unscented Kalman filter to fuse angular velocity, linear accelerometer, and magnetic field data via known kinematic relations between segments is presented.

Motion tracking and movement analysis applications based on IMU require attachment of sensing units onto body (human and robot) segments. When considering only rotational DoF, these segments can be connected by joints with one (e.g., pivot or hinge joint), two (e.g., saddle or condyloid joint), or three (e.g., spheroidal joint) DoF. The problem of calculating mechanism joint angles based on IMU measurements is an inverse kinematic problem. IMUs typically consist of a triad of gyroscopes, a triad of accelerometers, and a triad of magnetometers. Thus, they enable measurement of three-DoF segment orientation in operational space. When considering body-segment orientation measurements with IMUs attached to each segment and segments are linked with joints that have less than three DoFs, the resulting system becomes overdetermined at each point in time. Namely, measurements outnumber the unknown quantities required to describe segment orientation in space. Only in the case of spheroidal joints, the number of measurements equals the number of unknown variables. Such situations (with one, two, or three-DoF joints) are usual in human motion tracking. The problem may be solved using weighted least squares to yield estimates of segment orientations based on IMU data [16]. The estimation algorithm typically requires the use of the left pseudoinverse matrix. This choice also allows a reduction of the effects of the measurement noise. The solution of the presented inverse kinematic problem considering the weighted least squares leads to the implementation of the algorithm based on the Moore–Penrose weighted left pseudoinverse [17] of the mechanism Jacobian matrix. The Jacobian pseudoinverse can then be used in a closed-loop algorithm for calculating mechanism joint angles from the orientation and angular velocity of IMU sensors with the same method as for calculating the inverse kinematics of the robot manipulator with Jacobian inverse.

This paper is structured as follows. Section II introduces the kinematic-model-based sensory fusion of magnetoinertial data with Jacobian Moore–Penrose weighted-left-pseudoinverse and Kalman-adaptive gain matrix based on principles of Invariant Extended Kalman filter. Section III compares the performance of the Magnetoinertial tracking based on JAcobian PseudoInverse (MIJAPI) approach against well-established sensory fusion concepts based on the Unscented Kalman filter. Benefits and limitations of the MIJAPI concept are analyzed in Section IV, and the main findings are summarized in Section V.

The fundamental idea and novelty of the presented method is that when there are more measurements available than there are DoF of the mechanism, redundant measurements and knowledge of the kinematics of the mechanism can be used to improve the estimation of joint angles in presence of measurement noise, artifacts, and disturbances. Main contributions and novelties of this paper are as follows.

1) Motion tracking algorithm based on the Moore–Penrose weighted left pseudoinverse of the mechanism Jacobian matrix.
2) Algorithm is presented for a general serial kinematic chain and is, therefore, applicable for both the human motion tracking as well as tracking of robotic mechanisms. This paper also presents an example application for the upper limb.
3) Use of redundant information from IMUs to improve the estimation of joint angles by reducing the following effects:
   a) measurement noise from sensors;
   b) external magnetic disturbances;
   c) misalignment of the sensors attached to the segments.
4) Algorithm utilizes gain matrix for correcting the estimated angles based on the followings:
   a) invariant extended Kalman filter scheme that takes into account geometric properties of the problem;
   b) adaptive algorithm that takes into account unmodeled disturbances.

II. METHODS

Consider a general serial mechanism with N revolute (hinge) joints, as shown in Fig. 1. More complex joints (e.g., spheroidal joint) can be represented as a series of revolute joints connected by links of zero length. Mechanism links are selectively equipped with sensors $\mathcal{S}_i$ that are IMUs consisting of a triad of accelerometers, a triad of gyroscopes, and a triad of magnetometers. All sensors form a set $\mathcal{S} = \{\mathcal{S}_i : i = 1 \ldots M \leq N\}$. The base of the mechanism (link 0 with the base coordinate frame $O_0 - x_0 y_0 z_0$) can be stationary or mobile. Sensor $\mathcal{S}_0$ is assumed to measure the base orientation. (If base is stationary, sensor $\mathcal{S}_0$ is not necessarily required; however, a one-time calibration is needed.) The goal is to compute the joint angles of the mechanism and find the optimal placement of sensors on the mechanism.

A. Forward Kinematic and Differential Kinematic Model

Considering the Denavit–Hartenberg notation [18], the orientation of the link j relative to the link $j - 1$ is defined as

$$\mathbf{R}_j^{j-1}(\vartheta_j) = \text{Rot}(\mathbf{z}_{j-1}, \boldsymbol{\vartheta}_j) \cdot \text{Rot}(\mathbf{x}_j, \alpha_j) \qquad (1)$$

where $\text{Rot}(,)$ represents a rotation matrix, ϑ_j represents the angle of rotation between the links j and $j - 1$, which is measured from $\mathbf{x}_{j-1}$ to $\mathbf{x}_j$, about the $\mathbf{z}_{j-1}$ vector, and α_j represents the angle measured about the $\mathbf{x}_j$-axis between the vectors $\mathbf{z}_{j-1}$ and $\mathbf{z}_j$. The orientation of the link j relative to the base frame $O_0 - x_0 y_0 z_0$ can be computed as

$$\mathbf{R}_j = \prod_{k=1}^{j} \mathbf{R}_k^{k-1}(\vartheta_k). \qquad (2)$$

Angular velocity of link j relative to the base and expressed in the base coordinate frame $O_0 - x_0 y_0 z_0$ can be computed as

This article has been accepted for inclusion in a future issue of this journal. Content is final as presented, with the exception of pagination.

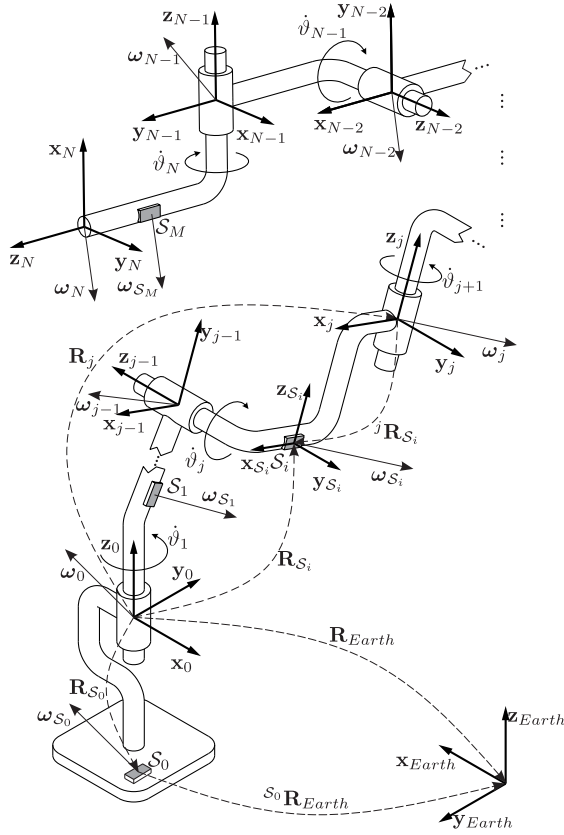MIHELJ *et al.*: SENSORY FUSION OF MAGNETOINERTIAL DATA

3

Fig. 1. General serial mechanism with revolute joints. Mechanism links are selectively equipped with sensors $\mathcal{S}_i$ being IMUs.

a function of joint velocities

$$\boldsymbol{\omega}_j = \sum_{k=1}^{j} \mathbf{z}_{k-1}\dot{\vartheta}_k = \begin{bmatrix} \mathbf{z}_0 & \dots & \mathbf{z}_{j-1} & \mathbf{0}^{3\times(N-j)} \end{bmatrix} \begin{bmatrix} \dot{\vartheta}_1 \\ \vdots \\ \dot{\vartheta}_N \end{bmatrix}$$

$$= \mathbf{J}_j \dot{\boldsymbol{\vartheta}} \qquad (3)$$

where $\mathbf{z}_{j-1}$ represents the joint axis vector that is given by the third column of the rotation matrix $\mathbf{R}_{j-1}$, whereas $\mathbf{z}_0 = \begin{bmatrix} 0 & 0 & 1 \end{bmatrix}^T$. Matrix $\mathbf{J}_j$ represents the Jacobian matrix for link j. All link velocities constitute the set

$$\Omega = \{\boldsymbol{\omega}_j : j = 1 \dots N\} \qquad (4)$$

with cardinality $N = |\Omega|$ (number of joint axes or links). Set Ω does not include base-link velocity. A totally ordered set of indices representing link velocities Ω can be determined as

$$\mathcal{N} = \{1, \dots, N\}. \qquad (5)$$

Consider a set of measurable link velocities (i.e., links that are equipped with sensors $\mathcal{S}_i$) as a subset of all link velocities

$$\Omega_{\mathcal{M}} \subseteq \Omega. \qquad (6)$$

Cardinality $M = |\Omega_{\mathcal{M}}|$ defines the number of measurable link velocities (without taking into account the base-link velocity). A totally ordered subset of indices defines the measurable link velocities

$$\mathcal{N} \supseteq \mathcal{M} = \{m_i : i = 1 \dots M\}. \qquad (7)$$

Meaning of subset $\mathcal{M}$ can be explained as follows: sensor $\mathcal{S}_i$ measures rotational velocity of link m_i, that is, $\boldsymbol{\omega}_{m_i}$.

Considering (3) and the set of measurable velocities (6), the following matrix equation can be defined:

$$\begin{bmatrix} \boldsymbol{\omega}_{m_1} \\ \vdots \\ \boldsymbol{\omega}_{m_M} \end{bmatrix} = \begin{bmatrix} \mathbf{J}_{m_1} \\ \vdots \\ \mathbf{J}_{m_M} \end{bmatrix} \dot{\boldsymbol{\vartheta}} \qquad (8)$$

and rewritten in a compact form as

$$\boldsymbol{\Omega}_{\mathcal{M}} = \boldsymbol{\mathcal{J}}_{\mathcal{M}} \dot{\boldsymbol{\vartheta}} \qquad (9)$$

where $\boldsymbol{\Omega}_{\mathcal{M}}$ represents a vector of all measurable link velocities and $\boldsymbol{\mathcal{J}}_{\mathcal{M}}$ is a block-triangular Jacobian matrix

$$\boldsymbol{\mathcal{J}}_{\mathcal{M}} = \begin{bmatrix} \boldsymbol{\mathcal{J}}_{\mathcal{M}_{11}} & \mathbf{0} & \mathbf{0} \\ \vdots & \ddots & \mathbf{0} \\ \boldsymbol{\mathcal{J}}_{\mathcal{M}_{11}} & \cdots & \boldsymbol{\mathcal{J}}_{\mathcal{M}_{MM}} \end{bmatrix} \qquad (10)$$

related to measurable link velocities. The rectangular (not necessarily square) submatrix $\boldsymbol{\mathcal{J}}_{\mathcal{M}_{ii}}$ of size $3 \times (m_i - m_{i-1})$ defines the following relation:

$$\boldsymbol{\omega}_{m_i} = \boldsymbol{\omega}_{m_{i-1}} + \boldsymbol{\mathcal{J}}_{\mathcal{M}_{ii}} \begin{bmatrix} \dot{\vartheta}_{m_{i-1}+1} \\ \vdots \\ \dot{\vartheta}_{m_i} \end{bmatrix} \qquad (11)$$

where $m_0 = 0$ ($\boldsymbol{\omega}_0 = \mathbf{0}$ if stationary base is assumed).

B. Jacobian Pseudoinverse-Based Inverse Kinematics

The inverse kinematics aim at computation of joint velocities and angles that correspond to the sensors angular velocities and orientations. Therefore, (9) must be inverted [19], leading to

$$\dot{\boldsymbol{\vartheta}} = \boldsymbol{\mathcal{J}}_{\mathcal{M}}^{\dagger} \boldsymbol{\Omega}_{\mathcal{M}} \qquad (12)$$

where $\dot{\boldsymbol{\vartheta}}$ is the optimal estimation of joint velocities in the least-square-error sense and $\boldsymbol{\mathcal{J}}_{\mathcal{M}}^{\dagger}$ is the Moore–Penrose left pseudoinverse of the Jacobian matrix $\boldsymbol{\mathcal{J}}_{\mathcal{M}}$ defined as

$$\boldsymbol{\mathcal{J}}_{\mathcal{M}}^{\dagger} = (\boldsymbol{\mathcal{J}}_{\mathcal{M}}^T \boldsymbol{\mathcal{J}}_{\mathcal{M}})^{-1} \boldsymbol{\mathcal{J}}_{\mathcal{M}}^T. \qquad (13)$$

The matrix $\boldsymbol{\mathcal{J}}_{\mathcal{M}}$ must have a full rank, which equals the number of joints N. The matrix can be rewritten as a product of an invertible matrix and a block-diagonal matrix with elements $\boldsymbol{\mathcal{J}}_{\mathcal{M}_{ii}}$

$$\boldsymbol{\mathcal{J}}_{\mathcal{M}} = \begin{bmatrix} \mathbf{I} & \mathbf{0} & \mathbf{0} \\ \vdots & \ddots & \mathbf{0} \\ \mathbf{I} & \cdots & \mathbf{I} \end{bmatrix} \begin{bmatrix} \boldsymbol{\mathcal{J}}_{\mathcal{M}_{11}} & \mathbf{0} & \mathbf{0} \\ \mathbf{0} & \ddots & \mathbf{0} \\ \mathbf{0} & \cdots & \boldsymbol{\mathcal{J}}_{\mathcal{M}_{MM}} \end{bmatrix} \qquad (14)$$

where $\mathbf{I}$ is an identity matrix of size 3×3. The rank of a square or rectangular matrix is not affected by left or right multiplication by an invertible matrix; the rank of a block-diagonal matrix equals the sum of the ranks of the matrices that are the main diagonal blocks, thus

$$\text{rank}(\boldsymbol{\mathcal{J}}_{\mathcal{M}}) = \sum_{i=1}^{M} \text{rank}(\boldsymbol{\mathcal{J}}_{\mathcal{M}_{ii}}). \qquad (15)$$

The matrix $\mathcal{J}_{\mathcal{M}}$ will have the full rank, if the following condition is satisfied:

$$\text{rank}(\mathcal{J}_{\mathcal{M}_{ii}}) = m_i - m_{i-1} \tag{16}$$

namely

$$\sum_{i=1}^{M}(m_i - m_{i-1}) = N \tag{17}$$

if we assume a measurable velocity of the last link in the chain. Condition (16) can only be satisfied by the correct placement of sensors $\mathcal{S}$. If the condition (16) is not satisfied, the placement of sensors is inadequate and availability of measurable link velocities is insufficient to estimate the angles of joint axes between links m_i and m_{i-1}. It is trivial to note that not more than three joint axes can be covered by a single sensor; an additional constraint is that the joint axes covered by a single sensor cannot be parallel. If this is the case, more sensors need to be added to the mechanism. When mechanism configuration approaches singularity, a damped least-squares inverse kinematics can be applied [20].

The solution in (13) assumes that all measurable link velocities $\mathbf{\Omega}_{\mathcal{M}}$ are equally weighted, meaning that all measurements are equally reliable. However, in a practical application, we might assume that certain measurements are less reliable than others. Consequently, a weighted left pseudoinverse Jacobian matrix can be computed as

$$\mathcal{J}_{\mathcal{M}}^{\dagger} = (\mathcal{J}_{\mathcal{M}}^{T}\mathbf{W}_{\mathcal{M}}^{-1}\mathcal{J}_{\mathcal{M}})^{-1}\mathcal{J}_{\mathcal{M}}^{T}\mathbf{W}_{\mathcal{M}}^{-1} \tag{18}$$

where $\mathbf{W}_{\mathcal{M}}$ is a weighting matrix (typically diagonal).

In (12), we assumed that measured link velocities are expressed in the base coordinate frame $O_0 - x_0 y_0 z_0$. However, this is usually not the case. Measurements are expressed in the body coordinate frame of the sensor. The orientation of the sensor $\mathcal{S}_i$, which is attached to the link m_i, in relation to the base frame $O_0 - x_0 y_0 z_0$ is

$$\mathbf{R}_{\mathcal{S}_i} = \mathbf{R}_{m_i}{}^{m_i}\mathbf{R}_{\mathcal{S}_i} \tag{19}$$

where rotation matrix ${}^{m_i}\mathbf{R}_{\mathcal{S}_i}$ represents orientation of the sensor $\mathcal{S}_i$ relative to the link m_i. Relation between the velocity expressed in the sensor body coordinate frame and the velocity expressed in the base frame is then

$$\boldsymbol{\omega}_{m_i} = \mathbf{R}_{\mathcal{S}_i}\boldsymbol{\omega}_{\mathcal{S}_i} \tag{20}$$

where $\boldsymbol{\omega}_{\mathcal{S}_i}$ is the rotational velocity as measured by the sensor $\mathcal{S}_i$ and expressed in the sensor body coordinate frame (for simplicity, we will not use the additional superscript $\mathcal{S}_i$). By rewriting (20) for all measurable velocities in a matrix form, we obtain

$$\begin{bmatrix} \boldsymbol{\omega}_{m_1} \\ \vdots \\ \boldsymbol{\omega}_{m_M} \end{bmatrix} = \begin{bmatrix} \mathbf{R}_{\mathcal{S}_1} & \cdots & \mathbf{0} \\ \mathbf{0} & \ddots & \mathbf{0} \\ \mathbf{0} & \cdots & \mathbf{R}_{\mathcal{S}_M} \end{bmatrix} \begin{bmatrix} \boldsymbol{\omega}_{\mathcal{S}_1} \\ \vdots \\ \boldsymbol{\omega}_{\mathcal{S}_M} \end{bmatrix}. \tag{21}$$

The above-mentioned relation can be compacted to

$$\mathbf{\Omega}_{\mathcal{M}} = \mathcal{R}_{\mathcal{S}}\mathbf{\Omega}_{\mathcal{S}} \tag{22}$$

where $\mathcal{R}_{\mathcal{S}}$ is a block-diagonal matrix having main diagonal blocks matrices $\mathbf{R}_{\mathcal{S}_i}$. By combining (9) and (22), the following relation can be written

$$\mathbf{\Omega}_{\mathcal{S}} = \mathcal{R}_{\mathcal{S}}^{T}\mathcal{J}_{\mathcal{M}}\dot{\boldsymbol{\vartheta}} = \mathcal{J}_{\mathcal{S}}\dot{\boldsymbol{\vartheta}} \tag{23}$$

where

$$\mathcal{J}_{\mathcal{S}} = \mathcal{R}_{\mathcal{S}}^{T}\mathcal{J}_{\mathcal{M}} \tag{24}$$

is the Jacobian matrix expressed in the sensor body coordinate frames. Matrix $\mathcal{R}_{\mathcal{S}}^{T}$ is invertible, thus $\text{rank}(\mathcal{J}_{\mathcal{S}}) = \text{rank}(\mathcal{J}_{\mathcal{M}})$.

The weighting matrix $\mathbf{W}_{\mathcal{M}}$ defines velocity weights relative to the base coordinate frame. If measured velocities are expressed in the sensor body coordinate frame, the following relation applies:

$$\mathbf{W}_{\mathcal{M}} = \mathcal{R}_{\mathcal{S}}\mathbf{W}_{\mathcal{S}}\mathcal{R}_{\mathcal{S}}^{T} \tag{25}$$

where $\mathbf{W}_{\mathcal{S}}$ is a weighting matrix related to velocities expressed in the sensor body coordinate frames. By combining (18), (24), and (25), the weighted left pseudoinverse Jacobian matrix can be rewritten as

$$\mathcal{J}_{\mathcal{M}}^{\dagger} = (\mathcal{J}_{\mathcal{S}}^{T}\mathbf{W}_{\mathcal{S}}^{-1}\mathcal{J}_{\mathcal{S}})^{-1}\mathcal{J}_{\mathcal{S}}^{T}\mathbf{W}_{\mathcal{S}}^{-1}\mathcal{R}_{\mathcal{S}}^{T}. \tag{26}$$

Equation (12) changes to

$$\dot{\boldsymbol{\vartheta}} = (\mathcal{J}_{\mathcal{S}}^{T}\mathbf{W}_{\mathcal{S}}^{-1}\mathcal{J}_{\mathcal{S}})^{-1}\mathcal{J}_{\mathcal{S}}^{T}\mathbf{W}_{\mathcal{S}}^{-1}\mathcal{R}_{\mathcal{S}}^{T}\mathbf{\Omega}_{\mathcal{M}}. \tag{27}$$

By defining the weighted left pseudoinverse Jacobian matrix related to the sensor body frame velocities as

$$\mathcal{J}_{\mathcal{S}}^{\dagger} = (\mathcal{J}_{\mathcal{S}}^{T}\mathbf{W}_{\mathcal{S}}^{-1}\mathcal{J}_{\mathcal{S}})^{-1}\mathcal{J}_{\mathcal{S}}^{T}\mathbf{W}_{\mathcal{S}}^{-1} \tag{28}$$

and considering (22), the following relation holds:

$$\dot{\boldsymbol{\vartheta}} = \mathcal{J}_{\mathcal{S}}^{\dagger}\mathbf{\Omega}_{\mathcal{S}}. \tag{29}$$

C. Prediction and Correction of the Estimated Joint Angles

The block scheme of the MIJAPI inverse kinematics approach is shown in Fig. 2.

The angular velocity measured by the sensor $\mathcal{S}_i$ (bar over the variable will be used throughout this paper to indicate measured quantities) equals

$$\bar{\boldsymbol{\omega}}_{\mathcal{S}_i} = \boldsymbol{\omega}_{\mathcal{S}_i} + \mathbf{b}_{\mathcal{S}_i} + \mathbf{w}_{\omega_{\mathcal{S}_i}} \tag{30}$$

where $\boldsymbol{\omega}_{\mathcal{S}_i}$ indicates the real sensor angular velocity and $\mathbf{b}_{\mathcal{S}_i}$ and $\mathbf{w}_{\omega_{\mathcal{S}_i}}$ represent the gyroscope bias and noise, respectively. With all measured velocities $\bar{\boldsymbol{\omega}}_{\mathcal{S}_i}$ combined into vector $\bar{\mathbf{\Omega}}_{\mathcal{S}}$, joint angular velocities can be computed as

$$\dot{\widehat{\boldsymbol{\vartheta}}} = \mathcal{J}_{\mathcal{S}}^{\dagger}\bar{\mathbf{\Omega}}_{\mathcal{S}}. \tag{31}$$

In theory, by integrating (31), joint angle predictions $\widehat{\boldsymbol{\vartheta}}$ can be computed as

$$\widehat{\boldsymbol{\vartheta}} = \widehat{\boldsymbol{\vartheta}}_0 + \int_0^t \dot{\widehat{\boldsymbol{\vartheta}}}dt. \tag{32}$$

However, due to the measurement noise, in particular, gyroscope bias $\mathbf{b}_{\mathcal{S}_i}$, in practical applications, this would only work for short time periods and exactly known initial joint positions $\widehat{\boldsymbol{\vartheta}}_0$.

This article has been accepted for inclusion in a future issue of this journal. Content is final as presented, with the exception of pagination.

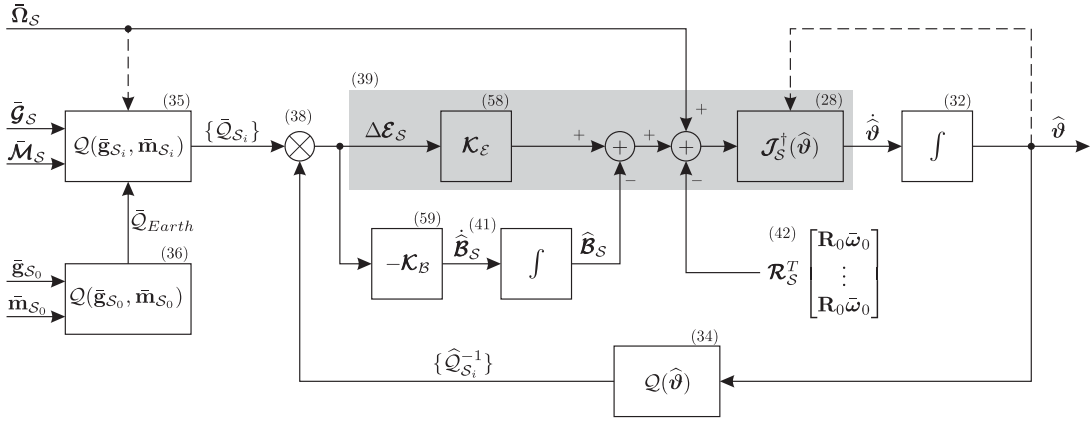MIHELJ *et al.*: SENSORY FUSION OF MAGNETOINERTIAL DATA

5

Fig. 2. Jacobian pseudoinverse-based inverse kinematics algorithm. Numbers in brackets denote the corresponding equations described in the text. Inputs into algorithm are all measured velocities $\bar{\omega}_{S_i}$ combined into vector $\bar{\Omega}_S$, all estimated static accelerations $\bar{g}_{S_i}$ [see (37)] combined into vector $\bar{\mathcal{G}}_S$, all measured magnetic field vectors $\bar{m}_{S_i}$ combined into vector $\bar{\mathcal{M}}_S$, and gravity vector $\bar{g}_{S_0}$ and earth magnetic field vector $\bar{m}_{S_0}$ in relation to the base frame O_0. Outputs from the algorithm are estimated joint angles $\widehat{\vartheta}$, which are calculated by integrating estimated joint velocities $\dot{\widehat{\vartheta}}$. Velocities $\dot{\widehat{\vartheta}}$ are calculated by using (39), by multiplying weighted left pseudoinverse Jacobian matrix $\mathcal{J}_S^\dagger$ and corrected measured velocities $(\bar{\Omega}_S + \mathcal{K}_\mathcal{E} \Delta \bar{\mathcal{E}}_S - \widehat{\mathcal{B}}_S)$. The term $\bar{\Omega}_S$ represents the feedforward path of the algorithm, and the term $\mathcal{K}_\mathcal{E} \Delta \bar{\mathcal{E}}_S - \widehat{\mathcal{B}}_S$ represents the feedback path of the algorithms.

The estimated sensor orientation $\widehat{\mathbf{R}}_{S_i} = \mathbf{R}_{S_i}(\widehat{\vartheta})$ in relation to the base coordinate frame $O_0 - x_0 y_0 z_0$ can be determined from (1), (2), and (19) by replacing ϑ_j with $\widehat{\vartheta}_j$

$$\widehat{\mathbf{R}}_{S_i} = \left(\prod_{j=1}^{m_i} \text{Rot}(\mathbf{z}_{j-1}, \widehat{\vartheta}_j) \cdot \text{Rot}(\mathbf{x}_j, \alpha_j) \right)^{m_i} \mathbf{R}_{S_i}. \quad (33)$$

The orientation matrix $\widehat{\mathbf{R}}_{S_i}$ can be expressed in terms of a quaternion $\widehat{\mathcal{Q}}_{S_i}$ as

$$\widehat{\mathcal{Q}}_{S_i} = \mathcal{Q}(\widehat{\mathbf{R}}_{S_i}). \quad (34)$$

Based on a triad of accelerometers, the sensor S_i measures a three-axial linear acceleration vector $\bar{\mathbf{a}}_{S_i}$, and based on a triad of magnetometers, the sensor S_i measures a three-axial magnetic field vector $\bar{\mathbf{m}}_{S_i}$. The two measured vectors, $\bar{\mathbf{a}}_{S_i}$ and $\bar{\mathbf{m}}_{S_i}$, both expressed in the sensor body coordinate frame, provide an estimate of the absolute sensor orientation in relation to the earth coordinate frame $O_\text{Earth} - x_\text{Earth} y_\text{Earth} z_\text{Earth}$. For simplicity, we assume that vectors $\bar{\mathbf{a}}_{S_i}$ and $\bar{\mathbf{m}}_{S_i}$ are normalized to the length 1 in static conditions. The q-method [21], [22] can be applied to compute the relative sensor orientation in terms of a quaternion $\mathcal{Q}(\bar{\mathbf{a}}_{S_i}, \bar{\mathbf{m}}_{S_i})$ representing the orientation of the earth coordinate frame in relation to the sensor body coordinate frame. The following sensor orientation in relation to the base coordinate frame $O_0 - x_0 y_0 z_0$ can then be obtained:

$$\bar{\mathcal{Q}}_{S_i} = \bar{\mathcal{Q}}_\text{Earth} (\mathcal{Q}(\bar{\mathbf{a}}_{S_i}, \bar{\mathbf{m}}_{S_i}))^{-1} \quad (35)$$

where the quaternion

$$\bar{\mathcal{Q}}_\text{Earth} = \mathcal{Q}(\mathbf{R}_{S_0}) \mathcal{Q}(\bar{\mathbf{a}}_{S_0}, \bar{\mathbf{m}}_{S_0}) \quad (36)$$

represents the orientation of the earth coordinate frame (defined by the gravity and magnetic field vectors) in relation to the base frame $O_0 - x_0 y_0 z_0$. The quaternion $\bar{\mathcal{Q}}_{S_i}$ is a measure of the absolute sensor S_i orientation and can be applied to correct the predicted signal $\widehat{\vartheta}$ values.

The computation of $\bar{\mathcal{Q}}_{S_i}$ is sensitive to dynamic acceleration components in $\bar{\mathbf{a}}_{S_i}$ and magnetic disturbances in $\bar{\mathbf{m}}_{S_i}$. The

effects of dynamic acceleration can be reduced by estimating the sensor S_i dynamic acceleration $\ddot{\widehat{\mathbf{p}}}_{S_i}$ from the estimated joint positions $\widehat{\vartheta}$, velocities $\dot{\widehat{\vartheta}}$ and accelerations $\ddot{\widehat{\vartheta}}$, and subtracting the estimated dynamic acceleration from the measured acceleration, thus obtaining only static acceleration (see Appendix A for more details on estimation of gravity and magnetic field vectors)

$$\bar{\mathbf{g}}_{S_i} = \bar{\mathbf{a}}_{S_i} - \ddot{\widehat{\mathbf{p}}}_{S_i}. \quad (37)$$

From (34), prediction of sensor orientation $\widehat{\mathcal{Q}}_{S_i}$ can be obtained from predicted joint angles $\widehat{\vartheta}$. The estimated absolute sensor orientation $\bar{\mathcal{Q}}_{S_i}$ is obtained from (35) by replacing $\bar{\mathbf{a}}_{S_i}$ with $\bar{\mathbf{g}}_{S_i}$. In ideal conditions, the two orientations would be equal. However, since this is not the case, the error quaternion $\Delta \bar{\mathcal{Q}}_{S_i}^{S_i} = \{\Delta \bar{\eta}_{S_i}, \Delta \bar{\epsilon}_{S_i}\}$ can be computed as

$$\Delta \bar{\mathcal{Q}}_{S_i}^{S_i} = \widehat{\mathcal{Q}}_{S_i}^{-1} \bar{\mathcal{Q}}_{S_i}. \quad (38)$$

The error quaternion $\Delta \bar{\mathcal{Q}}_{S_i}^{S_i}$ is expressed in the body coordinate frame of the estimated sensor orientation, $\Delta \bar{\eta}_{S_i}$ represents the quaternion scalar part, and $\Delta \bar{\epsilon}_{S_i}$ represents its vector part.

By taking into account the orientation estimation error $\Delta \bar{\epsilon}_{S_i}$ and the estimated gyroscope bias $\widehat{\mathbf{b}}_{S_i}$, (31) can be rewritten as

$$\dot{\widehat{\vartheta}} = \mathcal{J}_S^\dagger (\bar{\Omega}_S + \mathcal{K}_\mathcal{E} \Delta \bar{\mathcal{E}}_S - \widehat{\mathcal{B}}_S) \quad (39)$$

where $\mathcal{K}_\mathcal{E}$ is a positive-definite gain matrix

$$\Delta \bar{\mathcal{E}}_S = \begin{bmatrix} \Delta \bar{\epsilon}_{S_1} \\ \vdots \\ \Delta \bar{\epsilon}_{S_M} \end{bmatrix} \text{ and } \widehat{\mathcal{B}}_S = \begin{bmatrix} \widehat{\mathbf{b}}_{S_1} \\ \vdots \\ \widehat{\mathbf{b}}_{S_M} \end{bmatrix}. \quad (40)$$

The gyroscope bias can be estimated from the error vector $\Delta \bar{\mathcal{E}}_S$ with the following dynamics:

$$\dot{\widehat{\mathcal{B}}}_S = -\mathcal{K}_\mathcal{B} \Delta \bar{\mathcal{E}}_S. \quad (41)$$

In this case, we assumed that all sources off error can be attributed to gyroscope bias. This is not always necessarily

the case. Note that in (39)–(41), all values are expressed in the body coordinate frames of each particular sensor $\mathcal{S}_i$. If mechanism base link is not stationary, the vector $\bar{\mathbf{\Omega}}_{\mathcal{S}}$ in (39) must be replaced with

$$\bar{\mathbf{\Omega}}'_{\mathcal{S}} = \bar{\mathbf{\Omega}}_{\mathcal{S}} - \widehat{\mathcal{R}}_{\mathcal{S}}^T \begin{bmatrix} \mathbf{R}_0 \bar{\boldsymbol{\omega}}_0 \\ \vdots \\ \mathbf{R}_0 \bar{\boldsymbol{\omega}}_0 \end{bmatrix}. \tag{42}$$

D. Inverse Kinematics Kalman Gain Matrix

The dynamics of the orientation of the sensor $\mathcal{S}_i$ with noise entering the system can be described with equations

$$\dot{\mathcal{Q}}_{\mathcal{S}_i} = \frac{1}{2} \mathcal{Q}_{\mathcal{S}_i}[\boldsymbol{\omega}_{\mathcal{S}_i}] = \frac{1}{2} \mathcal{Q}_{\mathcal{S}_i}[\bar{\boldsymbol{\omega}}_{\mathcal{S}_i} - \mathbf{b}_{\mathcal{S}_i} - \mathbf{w}_{\omega_{\mathcal{S}_i}}] \tag{43}$$

$$\dot{\mathbf{b}}_{\mathcal{S}_i} = -\mathbf{w}_{\mathbf{b}_{\mathcal{S}_i}} \tag{44}$$

where $\mathcal{Q}_{\mathcal{S}_i}$ is the true orientation of the sensor $\mathcal{S}_i$ and $\mathbf{b}_{\mathcal{S}_i}$ is true gyroscope bias. Designation $[\mathbf{v}]$ represents a pure quaternion with a scalar part zero and a vector part $\mathbf{v}$. Vectors $\mathbf{w}_{\omega_{\mathcal{S}_i}}$ and $\mathbf{w}_{\mathbf{b}_{\mathcal{S}_i}}$ are uncorrelated Gaussian random vectors with zero means with covariance matrices

$$\mathbf{V}_{\omega_{\mathcal{S}_i}} = E\left(\mathbf{w}_{\omega_{\mathcal{S}_i}} \mathbf{w}_{\omega_{\mathcal{S}_i}}^T\right) \tag{45}$$

$$\mathbf{V}_{\mathbf{b}_{\mathcal{S}_i}} = E\left(\mathbf{w}_{\mathbf{b}_{\mathcal{S}_i}} \mathbf{w}_{\mathbf{b}_{\mathcal{S}_i}}^T\right). \tag{46}$$

Next, we build the nonlinear observer described by the following dynamics:

$$\dot{\widehat{\mathcal{Q}}}_{\mathcal{S}_i} = \frac{1}{2} \widehat{\mathcal{Q}}_{\mathcal{S}_i}[\bar{\boldsymbol{\omega}}_{\mathcal{S}_i} - \widehat{\mathbf{b}}_{\mathcal{S}_i} + \mathbf{K}_{\mathcal{Q}_{\mathcal{S}_i}} \Delta\bar{\boldsymbol{\epsilon}}_{\mathcal{S}_i}] \tag{47}$$

$$\dot{\widehat{\mathbf{b}}}_{\mathcal{S}_i} = -\mathbf{K}_{\mathbf{b}_{\mathcal{S}_i}} \Delta\bar{\boldsymbol{\epsilon}}_{\mathcal{S}_i} \tag{48}$$

where $\widehat{\mathcal{Q}}_{\mathcal{S}_i}$ is the estimated orientation of the sensor $\mathcal{S}_i$, $\widehat{\mathbf{b}}_{\mathcal{S}_i}$ is the estimated bias, and $\Delta\bar{\boldsymbol{\epsilon}}_{\mathcal{S}_i}$ is estimated error vector of the sensor $\mathcal{S}_i$.

Let us now write an error system

$$\Delta\mathcal{Q}_{\mathcal{S}_i}^{\mathcal{S}_i} = \widehat{\mathcal{Q}}_{\mathcal{S}_i}^{-1} \mathcal{Q}_{\mathcal{S}_i} \tag{49}$$

$$\Delta\mathbf{b}_{\mathcal{S}_i} = \mathbf{b}_{\mathcal{S}_i} - \widehat{\mathbf{b}}_{\mathcal{S}_i}. \tag{50}$$

After a short derivation given in Appendix B and combining (70) and (71) into matrix form of the system error dynamics, we arrive to

$$\begin{bmatrix} \Delta\dot{\boldsymbol{\epsilon}}_{\mathcal{S}_i} \\ \Delta\dot{\mathbf{b}}_{\mathcal{S}_i} \end{bmatrix} = (\mathbf{A}_{\mathcal{S}_i} - \mathbf{K}_{\mathcal{S}_i}\mathbf{C}) \begin{bmatrix} \Delta\boldsymbol{\epsilon}_{\mathcal{S}_i} \\ \Delta\mathbf{b}_{\mathcal{S}_i} \end{bmatrix} - \mathbf{w}_{\mathcal{S}_i} - \mathbf{K}_{\mathcal{S}_i}\mathbf{w}_{\Delta\boldsymbol{\epsilon}_{\mathcal{S}_i}} \tag{51}$$

where

$$\mathbf{A}_{\mathcal{S}_i} = \begin{bmatrix} -\mathbf{S}(\widehat{\boldsymbol{\omega}}_{\mathcal{S}_i}) & -\frac{1}{2}\mathbf{I} \\ \mathbf{0} & \mathbf{0} \end{bmatrix}, \quad \mathbf{C} = \begin{bmatrix} \mathbf{I} & \mathbf{0} \end{bmatrix}$$

$$\mathbf{K}_{\mathcal{S}_i} = \begin{bmatrix} \mathbf{K}_{\mathcal{Q}_{\mathcal{S}_i}} \\ -\mathbf{K}_{\mathbf{b}_{\mathcal{S}_i}} \end{bmatrix}$$

$$\mathbf{V}_{\mathcal{S}_i} = \begin{bmatrix} \mathbf{V}_{\omega_{\mathcal{S}_i}} & \mathbf{0} \\ \mathbf{0} & \mathbf{V}_{\mathbf{b}_{\mathcal{S}_i}} \end{bmatrix}, \quad \mathbf{w}_{\mathcal{S}_i} = \begin{bmatrix} \mathbf{w}_{\omega_{\mathcal{S}_i}} \\ \mathbf{w}_{\mathbf{b}_{\mathcal{S}_i}} \end{bmatrix}. \tag{52}$$

Equation (51) has the form of a linear equation of the state estimation error in the Kalman filter scheme, allowing

us to utilize the Kalman filter algorithm to calculate the gain matrix $\mathbf{K}_{\mathcal{S}_i}$

$$\mathbf{K}_{\mathcal{S}_i} = \mathbf{P}_{\mathcal{S}_i} \mathbf{C}^T \mathbf{V}_{\Delta\boldsymbol{\epsilon}_{\mathcal{S}_i}}^{-1} \tag{53}$$

where $\mathbf{P}_{\mathcal{S}_i}$ is calculated from

$$\dot{\mathbf{P}}_{\mathcal{S}_i} = \mathbf{A}_{\mathcal{S}_i}\mathbf{P}_{\mathcal{S}_i} + \mathbf{P}_{\mathcal{S}_i}\mathbf{A}_{\mathcal{S}_i}^T + \mathbf{V}_{\mathcal{S}_i} - \mathbf{K}_{\mathcal{S}_i}\mathbf{V}_{\Delta\boldsymbol{\epsilon}_{\mathcal{S}_i}}\mathbf{K}_{\mathcal{S}_i}^T. \tag{54}$$

We have arrived to this scheme by first computing the error term $\widehat{\mathcal{Q}}_{\mathcal{S}_i}^{-1} \mathcal{Q}_{\mathcal{S}_i}$, which does not violate the geometry of the quaternion space and quaternion multiplication and also preserves the unit norm. The error dynamics equations are then linearized around the equilibrium point, which leads us to the Kalman filter scheme. This is the typical approach adopted by the invariant extended Kalman filter scheme [8].

Kalman filter requires complete *a priori* knowledge about the measurement noise [23]–[25], which is usually determined off-line on preliminary measurements. However, if the noise statistics changes during the estimation, noise covariance matrix needs to be adapted during the estimation [24]. Due to the unmodeled disturbances in the magnetometer and accelerometer measurements, a model should take into account the unmodeled disturbances and adapt the covariance matrix $\mathbf{V}_{\Delta\boldsymbol{\epsilon}_{\mathcal{S}_i}}$. The covariance matrix $\mathbf{V}_{\Delta\boldsymbol{\epsilon}_{\mathcal{S}_i}}$ depends on the accelerometer and magnetometer noise covariance matrices $\mathbf{V}_a$ and $\mathbf{V}_m$, which can be estimated from the accelerometer and magnetometer measurement residuals using the maximum likelihood estimator. Matrix $\widehat{\mathbf{V}}_{\Delta\boldsymbol{\epsilon}_{\mathcal{S}_i}}$ is the statistical sample variance estimate of the $\mathbf{V}_{\Delta\boldsymbol{\epsilon}_{\mathcal{S}_i}}$ [26]

$$\widehat{\mathbf{V}}_{\Delta\boldsymbol{\epsilon}_{\mathcal{S}_i}} = \Xi(\Delta\bar{\eta}_{\mathcal{S}_i}, \Delta\bar{\boldsymbol{\epsilon}}_{\mathcal{S}_i})(\widehat{\mathbf{V}}_a + \widehat{\mathbf{V}}_m)\Xi(\Delta\bar{\eta}_{\mathcal{S}_i}, \Delta\bar{\boldsymbol{\epsilon}}_{\mathcal{S}_i})^T. \tag{55}$$

Equation (53) for calculating the gain $\mathbf{K}_{\mathcal{S}_i}$ can be accordingly updated to form the adaptive version of the algorithm for calculating the gain $\mathbf{K}_{\mathcal{S}_i}$

$$\mathbf{K}_{\mathcal{S}_i} = \mathbf{P}\mathbf{C}^T \widehat{\mathbf{V}}_{\Delta\boldsymbol{\epsilon}_{\mathcal{S}_i}}^{-1}. \tag{56}$$

Next, gains $\mathbf{K}_{\mathcal{Q}_{\mathcal{S}_i}}$ and $\mathbf{K}_{\mathbf{b}_{\mathcal{S}_i}}$ are extracted from the gain matrix $\mathbf{K}_{\mathcal{S}_i}$ since

$$\mathbf{K}_{\mathcal{S}_i} = \begin{bmatrix} \mathbf{K}_{\mathcal{Q}_{\mathcal{S}_i}} \\ -\mathbf{K}_{\mathbf{b}_{\mathcal{S}_i}} \end{bmatrix}. \tag{57}$$

Gains $\mathcal{K}_{\mathcal{E}}$ and $\mathcal{K}_{\mathcal{B}}$, which appear in (40) and (41), are constructed by constructing block-diagonal matrices that have on the main diagonal gain matrices $\mathbf{K}_{\mathcal{Q}_{\mathcal{S}_i}}$ and $\mathbf{K}_{\mathbf{b}_{\mathcal{S}_i}}$ of all sensors $\mathcal{S}_i$ from a set $\mathcal{S} = \{\mathcal{S}_i : i = 1 \dots M \leq N\}$

$$\mathcal{K}_{\mathcal{E}} = \begin{bmatrix} \mathbf{K}_{\mathcal{Q}_{\mathcal{S}_1}} & \cdots & \mathbf{0} \\ \mathbf{0} & \ddots & \mathbf{0} \\ \mathbf{0} & \cdots & \mathbf{K}_{\mathcal{Q}_{\mathcal{S}_M}} \end{bmatrix} \tag{58}$$

$$\mathcal{K}_{\mathcal{B}} = \begin{bmatrix} \mathbf{K}_{\mathbf{b}_{\mathcal{S}_1}} & \cdots & \mathbf{0} \\ \mathbf{0} & \ddots & \mathbf{0} \\ \mathbf{0} & \cdots & \mathbf{K}_{\mathbf{b}_{\mathcal{S}_M}} \end{bmatrix}. \tag{59}$$
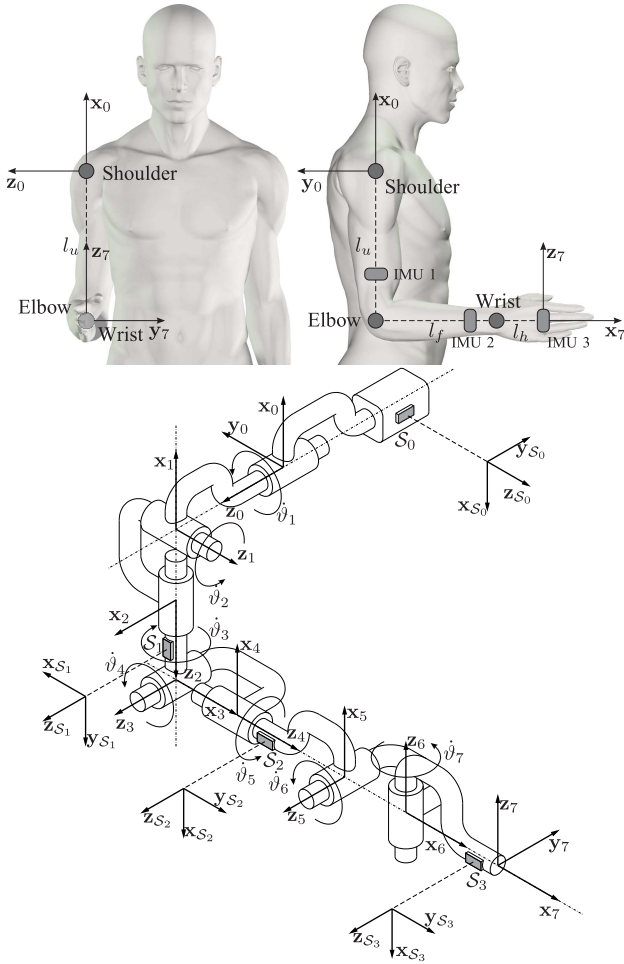
This article has been accepted for inclusion in a future issue of this journal. Content is final as presented, with the exception of pagination.

MIHELJ et al.: SENSORY FUSION OF MAGNETOINERTIAL DATA

7

Fig. 3. Human arm kinematic model. Mechanism links are selectively equipped with sensors $\mathcal{S}_i$ being IMUs.

III. RESULTS

The MIJAPI concept was validated on a kinematic model of a human arm, as shown in Fig. 3. The model consists of shoulder, elbow, and wrist joints connected by upper, forearm, and hand segments. The shoulder consists of three orthogonal revolute axes intersecting at the glenohumeral joint. The elbow consists of two revolute axes intersecting at the elbow joint. The wrist consists of two revolute axes intersecting at the wrist joint. In total, there are seven DoFs.

At least, three correctly placed IMUs are required for measurement of arm motion. For the particular case, the first IMU is placed on the upper arm close to the elbow joint (its displacement depends on all three shoulder DoFs), the second IMU is placed on the forearm at the wrist level (its displacement is additionally affected by both elbow DoF), and the third IMU is attached to the palm of the hand (its displacement depends on all arm DoF). With this configuration, rank($\mathcal{J}_{\mathcal{M}_{11}}(\vartheta_2 \neq \pm 90°)$) = 3, rank($\mathcal{J}_{\mathcal{M}_{11}}(\vartheta_2 = \pm 90°)$) = 2, rank($\mathcal{J}_{\mathcal{M}_{22}}$) = 2, and rank($\mathcal{J}_{\mathcal{M}_{33}}$) = 2. Thus, rank($\mathcal{J}_{\mathcal{M}}(\vartheta_2 \neq \pm 90°)$) = 7, whereas rank($\mathcal{J}_{\mathcal{M}}(\vartheta_2 = \pm 90°)$) = 6 with $\vartheta_2 = \pm 90°$ representing singular configuration. Near singularity, damped least-squares inverse Jacobian matrix was implemented [20].

The performance of the MIJAPI method with constant (CO) and Kalman-adapted (KA) gain matrix $\mathcal{K}_{\mathcal{E}}$ was validated in a simulation study by comparing estimated joint angles to: 1) separate Unscented Kalman filters for each IMU (K3) and 2) a single Unscented Kalman filter incorporating the arm model with seven DoFs (K1). Simulation signals were obtained by superimposing noise extracted from real IMUs on ideal values computed from the kinematic model of the human arm.

1) Ideal (noiseless) angular velocity, acceleration, and magnetic field values were determined from the model in Fig. 3 with prerecorded joint trajectories.
2) High-frequency noise was added to ideal signals.
3) Gyroscope signals were additionally compromised with real-sensor bias values and scaling factors on all axes.
4) Accelerometer signals were additionally disturbed with high-amplitude noise resulting from interactions of real IMUs with hard surface.
5) Magnetometer signals were manipulated with noise resulting from external magnetic fields.

Finally, displacement of the upper arm IMU was considered by rotating the device for 30° around the arm segment. Here, three additional cases were considered: 1) computation of arm angles based on the Moore–Penrose left pseudoinverse defined in (12); 2) Weighted left pseudoinverse as in (18); and 3) by using the error vector $\Delta \bar{\mathcal{E}}_{\mathcal{S}}$ for estimating IMU displacement. Analysis results are presented in Tables I and II in terms of signal-to-noise ratios (SNRs) for input and output signals (bold text indicates outputs with at least 15 dB SNR). SNR is defined as $\text{SNR} = 10 \log_{10}(A^2_{\text{signal}}/A^2_{\text{noise}})$, where A is root-mean-square amplitude. Noise is computed as a difference between ideal and corrupted input signals (angular velocity, acceleration, and magnetic field) or ideal and estimated (from corrupted inputs) output joint angles. SNR value is calculated for each signal. For input signals, mean, minimal, and maximal SNR values are computed for particular input modality from nine values (three IMUs with three axes each). SNR is calculated also for each of the seven joint angles. From this set of seven SNR values, mean, minimal, and maximal SNR values for joint angles are determined and shown in Tables I and II. Mean value of SNR values shows how method performs on average across a set of signals, minimal SNR value shows how method performs worst across a set of signals, and maximal SNR value shows how method performs best across a set of signals.

Independent Unscented Kalman filters demonstrate the best performance when noise is limited to individual IMUs. When disturbances have an affect across joints, the proposed concept based on the Jacobian pseudoinverse demonstrates the best performance. The worst performance was observed when using a single Unscented Kalman filter for the complete arm kinematics. The MIJAPI method (cases CO and KA) was the only one that guaranteed at least 15 dB SNR for all input conditions. In addition, the proposed method with constant gain matrix is approximately six times computationally more efficient than K3 method and 50 times more efficient than K1 method.

TABLE I

SNRs FOR MEASURED AND ESTIMATED SIGNALS ($\text{SNR}_{\widehat{\vartheta}}^{\text{CO}}$—CONSTANT GAINS, $\text{SNR}_{\widehat{\vartheta}}^{\text{KA}}$—KALMAN-ADAPTIVE GAINS, $\text{SNR}_{\widehat{\vartheta}}^{\text{K3}}$—THREE UNSCENTED KALMAN FILTERS, AND $\text{SNR}_{\widehat{\vartheta}}^{\text{K1}}$—ONE GENERAL UNSCENTED KALMAN FILTER) IN THE FORM $\frac{\text{mean}}{(\text{min,max})}$ FOR THE FOLLOWING CONDITIONS (DISTURBANCES ACCUMULATE): 1) NOISELESS MEASURED SIGNALS; 2) HIGH-FREQUENCY NOISE ON ALL SIGNALS; 3) GYRO BIAS AND SCALING; 4) DISTURBANCES ON ACCELEROMETERS (CONTACTS WITH HARD OBJECTS); AND 5) DISTURBANCES ON MAGNETOMETER (EXTERNAL MAGNETIC FIELD)

N	$\text{SNR}_{\bar{\omega}}$ (dB)	$\text{SNR}_{\bar{a}}$ (dB)	$\text{SNR}_{\bar{m}}$ (dB)	$\text{SNR}_{\widehat{\vartheta}}^{\text{CO}}$ (dB)	$\text{SNR}_{\widehat{\vartheta}}^{\text{KA}}$ (dB)	$\text{SNR}_{\widehat{\vartheta}}^{\text{K3}}$ (dB)	$\text{SNR}_{\widehat{\vartheta}}^{\text{K1}}$ (dB)
1	∞ (−,−)	∞ (−,−)	∞ (−,−)	33 (30,38)	31 (27,36)	34 (32,38)	24 (21,27)
2	63 (34,70)	46 (37,51)	43 (37,45)	29 (21,34)	28 (21,32)	33 (30,37)	24 (22,28)
3	28 (25,35)	46 (37,51)	43 (37,45)	24 (18,28)	23 (17,28)	29 (21,35)	18 (8,26)
4	28 (25,35)	16 (8,22)	43 (37,45)	24 (18,32)	24 (18,32)	24 (17,32)	16 (8,23)
5	28 (25,35)	16 (8,22)	17 (7,28)	19 (15,23)	19 (15,22)	16 (8,21)	16 (8,20)

TABLE II

SNRs FOR INPUT SIGNALS AS IN EXAMPLE 3 FROM TABLE I WITH ADDITIONAL 30° DISPLACEMENT OF THE UPPER ARM IMU FOR THE FOLLOWING CASES: 6) $\mathbf{W}_{\mathcal{M}}$ EQUAL TO IDENTITY MATRIX; 7) OPTIMIZED WEIGHTS $\mathbf{W}_{\mathcal{M}}$; AND 8) ESTIMATION OF IMU DISPLACEMENT FROM ERROR SIGNAL (NA—NOT APPLICABLE)

N	$\mathbf{W}_{\mathcal{M}}$	displacement	$\text{SNR}_{\widehat{\vartheta}}^{\text{CO}}$ (dB)	$\text{SNR}_{\widehat{\vartheta}}^{\text{KA}}$ (dB)	$\text{SNR}_{\widehat{\vartheta}}^{\text{K3}}$ (dB)	$\text{SNR}_{\widehat{\vartheta}}^{\text{K1}}$ (dB)
6	$\mathbf{W}_{\mathcal{M}} = \mathbf{I}$	not estimated	12 (4,23)	13 (6,22)	25 (1,35)	10 (3,22)
7	$\mathbf{W}_{\mathcal{M}} \neq \mathbf{I}$	not estimated	17 (11,24)	19 (12,25)	NA	NA
8	$\mathbf{W}_{\mathcal{M}} \neq \mathbf{I}$	estimated	21 (15,28)	22 (15,28)	NA	NA

Kalman gain matrices for MIJAPI method case KA are calculated using (53) from *a priori* state covariance matrix, measurement model matrix $\mathbf{C}$, and inverse of covariance matrix of the error term $\widehat{\mathbf{V}}_{\Delta\boldsymbol{\epsilon}_{\mathcal{S}_i}}$, resulting in adaptive algorithm for the calculation of the Kalman filter gains. Fig. 4(a) shows absolute value of the error term $\Delta\boldsymbol{\epsilon}_{\mathcal{S}_i}$ and a trace of the $\widehat{\mathbf{V}}_{\Delta\boldsymbol{\epsilon}_{\mathcal{S}_i}}$ matrix. Fig. 4(b) shows the Kalman gain $\mathbf{K}_{\mathcal{Q}_{\mathcal{S}}}$ used for updating the joint angles (see (39)). Fig. 4 shows that: 1) the Kalman gain matrix does not depend on the trajectory; 2) the diagonal terms (blue lines) have very similar values during the estimation; and 3) the off-diagonal terms (green line) are close to zero. For the first 5 s, the magnetoinertial unit is stationary, which is seen as phase with low noise. After that the unit is moved, which can be seen as the phase with increased noise [see Fig. 4(a)]. The source of the noise is primarily the translational acceleration. During that time the values of matrix $\widehat{\mathbf{V}}_{\Delta\boldsymbol{\epsilon}_{\mathcal{S}_i}}$ increase according to the increased noise present in error term and values of Kalman filter decrease. As a consequence, the noisy measurements have smaller effect on joint angles. Fig. 4(c) shows Kalman gain $\mathbf{K}_{\mathbf{b}_{\mathcal{S}}}$ for updating gyroscope biases (see (41)). Kalman gain $\mathbf{K}_{\mathbf{b}_{\mathcal{S}}}$ has large values in the beginning of the estimation to calculate the gyroscope biases, whereas during the increased measurement noise, the gain becomes small and the biases are not updated. In the last 5 s, the unit is again stationary and the noise level
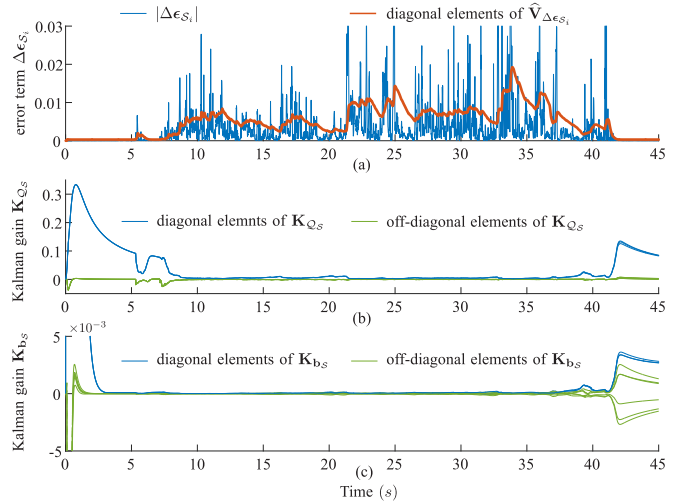

Fig. 4. (a) Absolute value of the error term $\Delta\boldsymbol{\epsilon}_{\mathcal{S}_i}$ (blue line) from which the covariance matrix $\widehat{\mathbf{V}}_{\Delta\boldsymbol{\epsilon}_{\mathcal{S}_i}}$ (diagonal terms of matrix are shown in red line) is calculated. (b) Kalman gain $\mathbf{K}_{\mathcal{Q}_{\mathcal{S}}}$ for updating the joint angles. (c) Kalman gain $\mathbf{K}_{\mathbf{b}_{\mathcal{S}}}$ for updating the gyroscope biases.

becomes small, the values of the Kalman gain $\mathbf{K}_{\mathbf{b}_{\mathcal{S}}}$ again increase to improve the estimation of gyroscope biases using the measurements.

Fig. 5 presents an example of measured human upper limb trajectory in terms of seven joint angles (shoulder flexion/extension, shoulder abduction/adduction, shoulder internal/external rotation, elbow flexion/extension, wrist pronatoin/supination, wrist ulnar/radial deviation, and wrist flexion extension). Joint angles estimated from IMU data are compared to values obtained from an optical tracking system. In order to demonstrate worst case scenario (condition 8 in Table II), all IMU data were additionally corrupted with acceleration and magnetic disturbances (extracted from real IMU data obtained separately), and upper arm sensor was virtually rotated about its y-axis for 30°. The MIJAPI method with constant gains (CO) was used. The system demonstates the excellent estimation performance also in conditions with significant disturbances.

IV. DISCUSSION

Results presented in Table I show that methods CO, KA, and K3 perform comparably in conditions 1 to 4, while in condition 5 the methods CO and KA perform better than the methods K3 and K1. Note that SNR of 20 dB corresponds to 1% of error, and SNR of 15 dB corresponds to 3% of error. Results presented in Table II imply that K3 performs best since the average SNR is high (25 dB); however, when evaluating the performance of the method, both average as well as minimal SNR need to be taken into account. While for one method, average SNR can be high, which means that, in average, estimation of the angles is very good for this method, one of the estimated angles can be estimated poorly. This is the case for K3 method since the minimum SNR is only 1 dB, which means that one of the angles drifts away considerably from the actual angle values. This is undesirable performance even though average SNR is high. While for the

This article has been accepted for inclusion in a future issue of this journal. Content is final as presented, with the exception of pagination.

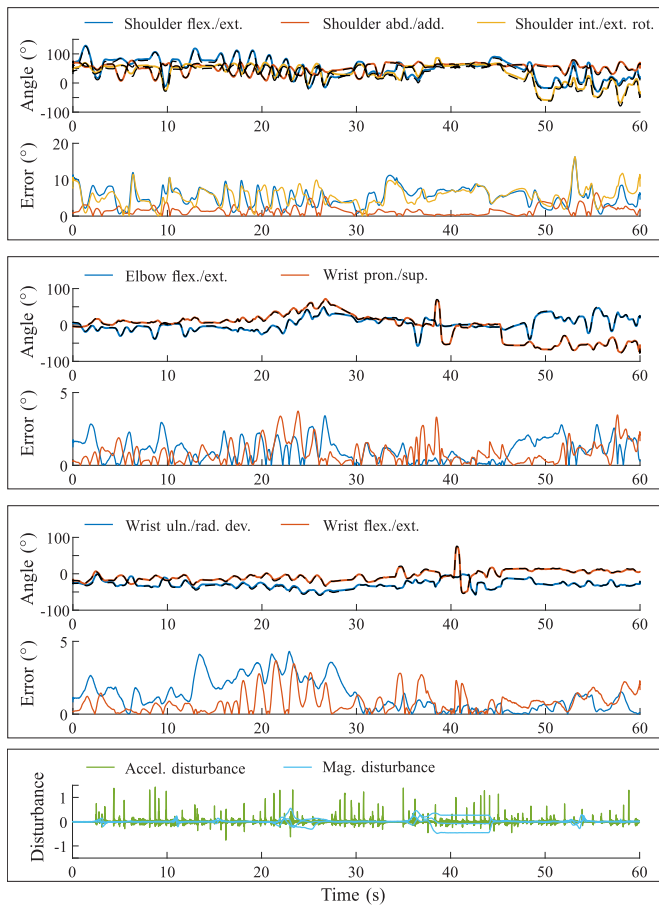MIHELJ *et al.*: SENSORY FUSION OF MAGNETOINERTIAL DATA

9

Fig. 5. Estimated trajectories from IMUs and trajectories from optical tracking system (superimposed black dashed lines) for seven arm angles. For each pair of estimated and measured trajectories, the error signal is shown. To demonstrate worst case scenario, IMU signals were additionally corrupted with acceleration and magnetic disturbances (extracted from real IMU data) as indicated in the last subplot (normalized amplitude, example for upper arm IMU).

CO and KA methods in condition 8 in Table II, the average SNR is slightly lower than for the K3 method, the minimum SNR is considerably better, and none of the angles drifts away. In conditions 1–5, the KA method performs slightly worse than the CO method, whereas in conditions 6–8, it performs slightly better. However, the differences are minimal, and from the practical point of view, the performance is the same.

Main causes of uncertainty are sensor noise (high-frequency noise), sensor bias and drift, scaling errors, human motion artifacts, magnetic disturbances, and displacement of sensors in relation to the segment. Condition 1 in Table I shows the performance results for signals without disturbances. Disturbances are then added step by step in conditions 2–5. Sensor noise (condition 2 in Table I) does not degrade the performance significantly. In addition of gyro bias, drift and scaling errors significantly affect all methods as shown by average drop of 12 dB of minimal value of SNR compared to condition 3. Gyro bias can be easily estimated and removed prior to joint angle estimation by calibrating the gyro sensor [1], [14], while gyro drift needs to be estimated online [see (41)]. Addition of disturbances of accelerometers does not degrade the performance of the methods since they are

short (for example, see bottom figure of disturbances in Fig. 5) and can be compensated by gyroscope measurements. Biases and scaling errors of accelerometers can also be reduced by calibrating the accelerometers [27]. Addition of magnetic disturbances affects the performance of K3 method significantly, while performance of the K1 has already been significantly affected by gyro drift and scaling errors. MIJAPI method is also affected by magnetic disturbances, however, to lesser degree by about 3 dB, to about same level as an addition of gyro drift and scaling errors. Magnetic disturbances due to sources on the IMU unit itself can be reduced significantly by proper calibration [28], while magnetic disturbances coming from the environment can be reduced by estimation and compensation of the magnetic disturbance during joint angle estimation [29] or by avoiding the environment with magnetic disturbances. Table II (condition 6) shows the effect of displacement of the IMU sensor by 30°. Displacement affects all methods significantly. With MIJAPI method, this can be reduced in two ways: first, by giving less weight to the displaced IMU (see condition 7 in Table II), and second, by estimating the displacement of the IMU (see condition 8 in Table II). One of the main advantages of the MIJAPI method is the use of the redundant information from IMUs to improve the estimation of joint angles by reducing the effect of misalignment of the sensors attached to the segments. MIJAPI method uses redundant data to estimate the displacement. Estimation reduces the effect of displacement significantly (see condition 8 in Table II). Alternatively, displacement can be estimated prior the actual experiments by performing predefined calibration motions [30].

UKF Kalman filters in the method K1 and the method K3 use different processes and measurement models. Method K3 uses three separate Kalman filters that estimate the orientation of each IMU independently. The angles are then calculated from the estimated orientations of arm segments. The Kalman filter in method K1 includes a complete kinematic model of the arm and estimates angles directly. The filter K1 performs worst of the three methods in conditions 1–5 shown in Table I. It performs better in conditions 6 (see Table II; here, we refer to minimal SNR not to average SNR), where the advantage of the full kinematic model is finally seen.

The main reason for poorer performance is that the state vector of the Kalman filter used in the method K1 consists of two types of variables: joint angles that are defined in joint space and gyroscope biases that are defined in body frame of each magnetoinertial unit. *A posteriori* state estimate is calculated from *a priori* state estimate, Kalman gain, and measurement model error, and the relation between the error and the *a posteriori* state is linear. This mixture of types of states in one state vector and the fact that the relation between the state and the error is linear poses a question, in which space should the error be expressed since it can only be expressed in one of the two spaces. One of the types of states will therefore be updated with correction expressed in different space, and it will be corrected in nonoptimal way. While the vector part of the error quaternion is related to rotational velocity and is therefore expressed in the body frame, it can be mapped into joint space by using the Jacobian matrix.

The experiments have shown that K1 performs better when the error is mapped in joint space. This weakness of mixed types of states in the classical Kalman filter was also one of the reasons to develop the MIJAPI algorithm that takes into account the geometrical properties of the serial mechanism kinematics. In the proposed method based on Invariant filters, the Kalman gain is multiplied directly with the vector part of the error quaternion; however, the update for the estimation of the *a posteriori* joint angles is then mapped from the body frame into joint space, where the *a priori* joint angles states are updated. As a result, the performance of the CO and KA methods is considerably better compared to K1 method in conditions 3–5.

V. CONCLUSION

This paper presents the novel algorithm for estimation of joint angles based on magnetoinertial measurements. The estimation requires the complete kinematic model of the system, including constraints introduced by various types of rotational joints. The computation is based on the Moore–Penrose left pseudoinverse of the system Jacobian matrix that relates segment angular velocities to joint velocities and presents the weighted least-squares solution to the problem. Measured segment angular velocities are used as a feedforward term, while the estimation error multiplied by a constant or Kalman-adaptive gain matrix is used in a feedback loop. The estimation error is represented by the error quaternion computed from the estimated segment orientation and the segment orientation determined from acceleration and magnetometer data. The two measurements are susceptible to various disturbances (e.g., dynamic accelerations and external magnetic fields), which can be reduced through signal preprocessing.

The results of the experimental validation demonstrate that the MIJAPI algorithm is capable to assess joint angles of the upper limb in the presence of various disturbances. The output is not susceptible to signal drift. The MIJAPI algorithm is computationally more efficient than the corresponding solutions based on the Kalman filter. However, the Kalman filter was found to perform slightly better in conditions without significant disturbances or kinematic misalignments. The method with the Kalman-adaptive gains performs better than the solution with constant gain matrix in the worst case scenarios in terms of disturbances.

The MIJAPI method is applicable in areas of human motion tracking and analysis as well as robotics, where orientation estimation of serially linked segments with rotational joints is of interest.

APPENDIX A
ESTIMATION OF GRAVITY AND MAGNETIC FIELD VECTORS

Dynamic acceleration $\ddot{\bar{\mathbf{p}}}_{\mathcal{S}_i}$ acting on the sensor $\mathcal{S}_i$ can be calculated using the following approach. The sensor $\mathcal{S}_i$ is attached to the link $j = m_i$

$$\ddot{\bar{\mathbf{p}}}_{\mathcal{S}_i} = {}^j\widehat{\mathbf{R}}_{\mathcal{S}_i}\left(\ddot{\bar{\mathbf{p}}}_j^j + \hat{\dot{\boldsymbol{\omega}}}_j^j \times \mathbf{r}_{j,\mathcal{S}_i}^j + \widehat{\boldsymbol{\omega}}_j^j \times \left(\widehat{\boldsymbol{\omega}}_j^j \times \mathbf{r}_{j,\mathcal{S}_i}^j\right)\right) \quad (60)$$

where $\mathbf{r}_{j,\mathcal{S}_i}^j$ is the position of the sensor $\mathcal{S}_i$ relative to the coordinate frame j attached to the link j, $\ddot{\bar{\mathbf{p}}}_j^j$, $\hat{\dot{\boldsymbol{\omega}}}_j^j$, and $\widehat{\boldsymbol{\omega}}_j^j$ are dynamic acceleration, angular acceleration, and angular velocity of the link j relative to the link coordinate frame, respectively. Angular velocity $\widehat{\boldsymbol{\omega}}_j$ can be computed directly using (3)

$$\widehat{\boldsymbol{\omega}}_j = \sum_{k=1}^{j} \mathbf{z}_{k-1}(\widehat{\boldsymbol{\vartheta}})\,\hat{\dot{\vartheta}}_k = \mathbf{J}_j(\widehat{\boldsymbol{\vartheta}})\,\hat{\dot{\boldsymbol{\vartheta}}}. \quad (61)$$

Angular velocity in (61) is expressed relative to the base frame and needs to be transformed into the link frame

$$\widehat{\boldsymbol{\omega}}_j^j = \widehat{\mathbf{R}}_{\mathcal{S}_i}^T\widehat{\boldsymbol{\omega}}_j. \quad (62)$$

Angular acceleration $\hat{\dot{\boldsymbol{\omega}}}_j^j$ and dynamic acceleration $\ddot{\bar{\mathbf{p}}}_j^j$ of the link j relative to the coordinate frame of the link j can be computed iteratively using the Newton–Euler approach

$$\hat{\dot{\boldsymbol{\omega}}}_j^j = {}^{j-1}\widehat{\mathbf{R}}_j^T\left(\hat{\dot{\boldsymbol{\omega}}}_{j-1}^{j-1} + \ddot{\hat{\vartheta}}_j\mathbf{z}_0 + \dot{\hat{\vartheta}}_j\widehat{\boldsymbol{\omega}}_{j-1}^{j-1} \times \mathbf{z}_0\right) \quad (63)$$

$$\ddot{\bar{\mathbf{p}}}_j^j = {}^{j-1}\widehat{\mathbf{R}}_j^T\,\ddot{\bar{\mathbf{p}}}_{j-1}^{j-1} + \hat{\dot{\boldsymbol{\omega}}}_j^j \times \mathbf{r}_{j-1,j}^j + \widehat{\boldsymbol{\omega}}_j^j \times \left(\widehat{\boldsymbol{\omega}}_j^j \times \mathbf{r}_{j-1,j}^j\right) \quad (64)$$

where $\mathbf{r}_{j-1,j}^j$ is a vector pointing from the coordinate frame of link $j-1$ to the coordinate frame of link j expressed in the coordinate frame of link j.

Computationally more efficient is direct approximation of the static acceleration $\bar{\mathbf{g}}_{\mathcal{S}_i}$. The updated static acceleration $\bar{\mathbf{g}}_{\mathcal{S}_i}^+$ is obtained by rotating the previous static acceleration estimate $\bar{\mathbf{g}}_{\mathcal{S}_i}^-$ for a small angle $\bar{\omega}_{\mathcal{S}_i}dt$. The integration drift can be compensated by taking into account the measured acceleration vector $\bar{\mathbf{a}}_{\mathcal{S}_i}$. The corrected rotation angle is then

$$d\boldsymbol{\varphi} = \bar{\omega}_{\mathcal{S}_i}dt + \mathbf{K}_g(\|\bar{\mathbf{a}}_{\mathcal{S}_i}\|)\left(\frac{\bar{\mathbf{a}}_{\mathcal{S}_i}}{\|\bar{\mathbf{a}}_{\mathcal{S}_i}\|} \times \bar{\mathbf{g}}_{\mathcal{S}_i}^-\right) \quad (65)$$

where $\mathbf{K}_g(\|\bar{\mathbf{a}}_{\mathcal{S}_i}\|)$ is an adaptive feedback gain value that reflects quality of the measured acceleration (e.g., acceleration norm). The new estimated acceleration is then

$$\bar{\mathbf{g}}_{\mathcal{S}_i}^+ = (\mathbf{I} - \mathbf{S}(d\boldsymbol{\varphi}))\bar{\mathbf{g}}_{\mathcal{S}_i}^- \quad (66)$$

where $\mathbf{I}$ is an identity matrix and $\mathbf{S}(\cdot)$ is a skew-symmetric operator. Similar approach can be applied also for estimation of the magnetic field vector $\bar{\mathbf{m}}_{\mathcal{S}_i}$ in the case of short-term disturbances [31]. The adaptive feedback gain $\mathbf{K}_m$ must reflect changes in the norm of the measured magnetic field vector $\|\bar{\mathbf{m}}_{\mathcal{S}_i}\|$ and the changes in the magnetic dip angle.

APPENDIX B
DERIVATION OF THE SYSTEM ERROR DYNAMICS

The dynamics of the error system are

$$\Delta\dot{\mathcal{Q}}_{\mathcal{S}_i}^{\mathcal{S}_i} = \frac{d}{dt}\left(\widehat{\mathcal{Q}}_{\mathcal{S}_i}^{-1}\mathcal{Q}_{\mathcal{S}_i}\right) \quad (67)$$

$$= -\widehat{\mathcal{Q}}_{\mathcal{S}_i}^{-1}\dot{\widehat{\mathcal{Q}}}_{\mathcal{S}_i}\Delta\mathcal{Q}_{\mathcal{S}_i}^{\mathcal{S}_i} + \widehat{\mathcal{Q}}_{\mathcal{S}_i}^{-1}\dot{\mathcal{Q}}_{\mathcal{S}_i}. \quad (68)$$

This article has been accepted for inclusion in a future issue of this journal. Content is final as presented, with the exception of pagination.

MIHELJ *et al.*: SENSORY FUSION OF MAGNETOINERTIAL DATA

11

By combining (43), (47), and (68) and after some tedious but simple computation, we arrive to the following system:

$$\Delta \dot{\mathcal{Q}}_{\mathcal{S}_i}^{\mathcal{S}_i} = -(\bar{\boldsymbol{\omega}}_{\mathcal{S}_i} - \widehat{\mathbf{b}}_{\mathcal{S}_i}) \times \Delta \boldsymbol{\epsilon}_{\mathcal{S}_i} - \frac{1}{2} \Delta \mathcal{Q}_{\mathcal{S}_i}^{\mathcal{S}_i} [\Delta \mathbf{b}_{\mathcal{S}_i}]$$
$$- \Delta \mathcal{Q}_{\mathcal{S}_i}^{\mathcal{S}_i} [\mathbf{w}_{\omega_{\mathcal{S}_i}}] - [\mathbf{K}_{\mathcal{Q}_{\mathcal{S}_i}} (\Delta \boldsymbol{\epsilon}_{\mathcal{S}_i} + \mathbf{w}_{\Delta \boldsymbol{\epsilon}_{\mathcal{S}_i}})] \Delta \mathcal{Q}_{\mathcal{S}_i}^{\mathcal{S}_i}. \quad (69)$$

We now linearize the error system around $\Delta \mathcal{Q}_{\mathcal{S}_i}^{\mathcal{S}_i} = [1, 0, 0, 0]^T$ and $\Delta \mathbf{b}_{\mathcal{S}_i} = [0, 0, 0]^T$ and drop the quadratic terms and infinitesimal state error, which leads to the system

$$\Delta \dot{\boldsymbol{\epsilon}}_{\mathcal{S}_i} = -\widehat{\boldsymbol{\omega}}_{\mathcal{S}_i} \times \Delta \boldsymbol{\epsilon}_{\mathcal{S}_i} - \frac{1}{2} \Delta \mathbf{b}_{\mathcal{S}_i} - \mathbf{w}_{\omega_{\mathcal{S}_i}}$$
$$- \mathbf{K}_{\mathcal{Q}_{\mathcal{S}_i}} \Delta \boldsymbol{\epsilon}_{\mathcal{S}_i} - \mathbf{K}_{\mathcal{Q}_{\mathcal{S}_i}} \mathbf{w}_{\Delta \boldsymbol{\epsilon}_{\mathcal{S}_i}} \quad (70)$$

$$\Delta \dot{\mathbf{b}}_{\mathcal{S}_i} = -\mathbf{w}_{\mathbf{b}_{\mathcal{S}_i}} + \mathbf{K}_{\mathbf{b}_{\mathcal{S}_i}} \Delta \boldsymbol{\epsilon}_{\mathcal{S}_i} + \mathbf{K}_{\mathbf{b}_{\mathcal{S}_i}} \mathbf{w}_{\Delta \boldsymbol{\epsilon}_{\mathcal{S}_i}} \quad (71)$$

where $\bar{\boldsymbol{\omega}}_{\mathcal{S}_i} - \widehat{\mathbf{b}}_{\mathcal{S}_i}$ has been replaced with $\widehat{\boldsymbol{\omega}}_{\mathcal{S}_i}$.

REFERENCES

[1] I. H. López-Nava and A. Muñoz-Meléndez, "Wearable inertial sensors for human motion analysis: A review," *IEEE Sensors J.*, vol. 16, no. 22, pp. 7821–7834, Nov. 2016.

[2] E. Rocon, J. C. Moreno, A. F. Ruiz, F. Brunetti, J. A. Miranda, and J. L. Pons, "Application of inertial sensors in rehabilitation robotics," in *Proc. IEEE 10th Int. Conf. Rehabil. Robot.*, Jun. 2007, pp. 145–150.

[3] J. A. Corrales, G. J. G. Gómez, F. Torres, and V. Perdereau, "Cooperative tasks between humans and robots in industrial environments," *Int. J. Adv. Robot. Syst.*, vol. 9, no. 94, pp. 1–10, 2012.

[4] M. Saha, R. Ghosh, and B. Goswami, "Robustness and sensitivity metrics for tuning the extended Kalman filter," *IEEE Trans. Instrum. Meas.*, vol. 63, no. 4, pp. 964–971, Apr. 2014.

[5] E. Kraft, "A quaternion-based unscented Kalman filter for orientation tracking," in *Proc. 6th Int. Conf. Inf. Fusion*, vol. 1, 2003, pp. 47–54.

[6] R. Mahony, T. Hamel, and J.-M. Pflimlin, "Nonlinear complementary filters on the special orthogonal group," *IEEE Trans. Autom. Control*, vol. 53, no. 5, pp. 1203–1218, Jun. 2008.

[7] X. Yun and E. R. Bachmann, "Design, implementation, and experimental results of a quaternion-based Kalman filter for human body motion tracking," *IEEE Trans. Robot.*, vol. 22, no. 6, pp. 1216–1227, Dec. 2006.

[8] P. Martin and E. Salaün, "Generalized multiplicative extended Kalman filter for aided attitude and heading reference system," in *Proc. AIAA Guid., Navigat., Control Conf.*, 2010, p. 8300.

[9] S. Bonnabel, P. Martin, and P. Rouchon, "Non-linear symmetry-preserving observers on Lie groups," *IEEE Trans. Autom. Control*, vol. 54, no. 7, pp. 1709–1713, Jul. 2009.

[10] H. Zhou and H. Hu, "Reducing drifts in the inertial measurements of wrist and elbow positions," *IEEE Trans. Instrum. Meas.*, vol. 59, no. 3, pp. 575–585, Mar. 2010.

[11] A. Young, "Use of body model constraints to improve accuracy of inertial motion capture," in *Proc. Int. Conf. Body Sensor Netw. (BSN)*, Jun. 2010, pp. 180–186.

[12] T. Seel, T. Schauer, and J. Raisch, "Joint axis and position estimation from inertial measurement data by exploiting kinematic constraints," in *Proc. IEEE Int. Conf. Control Appl. (CCA)*, Oct. 2012, pp. 45–49.

[13] T. Seel, J. Raisch, and T. Schauer, "IMU-based joint angle measurement for gait analysis," *Sensors*, vol. 14, no. 4, pp. 6891–6909, 2014.

[14] S. Šlajpah, R. Kamnik, and M. Munih, "Kinematics based sensory fusion for wearable motion assessment in human walking," *Comput. Methods Programs Biomed.*, vol. 116, no. 2, pp. 131–144, 2014.

[15] Z. Zhang, W. C. Wong, and J. Wu, "Wearable sensors for 3D upper limb motion modeling and ubiquitous estimation," *J. Control Theory Appl.*, vol. 9, no. 1, pp. 10–17, 2011.

[16] A. Ben-Israel and T. Greville, *Generalized Inverses—Theory and Applications*. New York, NY, USA: Springer-Verlag, 2003.

[17] B. Siciliano, L. Sciavicco, L. Villani, and G. Oriolo, *Robotics—Modelling, Planning and Control*. London, U.K.: Springer-Verlag, 2009, pp. 575–576.

[18] J. Denavit and R. S. Hartenberg, "A kinematic notation for lower-pair mechanisms based on matrices," *ASME J. Appl. Mech.*, vol. 23, pp. 215–221, Jun. 1955.

[19] C. D. Meyer, Jr., "Generalized inverses of block triangular matrices," *SIAM J. Appl. Math.*, vol. 19, no. 4, pp. 741–750, 1970.

[20] S. Chiaverini, B. Siciliano, and O. Egeland, "Review of the damped least-squares inverse kinematics with experiments on an industrial robot manipulator," *IEEE Trans. Control Syst. Technol.*, vol. 2, no. 2, pp. 123–134, Jun. 1994.

[21] P. Davenport, "A vector approach to the algebra of rotations with applications," NASA, Washington, DC, USA, Tech. Rep. X-546-65-437, 1965.

[22] F. L. Markley and D. Mortari, "Quaternion attitude estimation using vector observations," *J. Astron. Sci.*, vol. 48, no. 2, pp. 359–380, 2000.

[23] R. K. Mehra, "On the identification of variances and adaptive Kalman filtering," *IEEE Trans. Autom. Control*, vol. AC-15, no. 2, pp. 175–184, Apr. 1970.

[24] R. K. Mehra, "Approaches to adaptive filtering," *IEEE Trans. Autom. Control*, vol. AC-17, no. 5, pp. 693–698, Oct. 1972.

[25] T. Berry and T. Sauer, "Adaptive ensemble Kalman filtering of nonlinear systems," *Tellus A, Dyn. Meteorol. Oceanogr.*, vol. 65, no. 1, 2013, Art. no. 20331.

[26] D. Choukroun, I. Bar-Itzhack, and Y. Oshman, "Novel quaternion Kalman filter," *IEEE Trans. Aerosp. Electron. Syst.*, vol. 42, no. 1, pp. 174–190, Jan. 2006.

[27] T. Beravs, J. Podobnik, and M. Munih, "Three-axial accelerometer calibration using Kalman filter covariance matrix for online estimation of optimal sensor orientation," *IEEE Trans. Instrum. Meas.*, vol. 61, no. 9, pp. 2501–2511, Oct. 2012.

[28] T. Beravs, S. Begus, J. Podobnik, and M. Munih, "Magnetometer calibration using Kalman filter covariance matrix for online estimation of magnetic field orientation," *IEEE Trans. Instrum. Meas.*, vol. 63, no. 8, pp. 2013–2020, Aug. 2014.

[29] S. Šlajpah, R. Kamnik, and M. Munih, "Compensation for magnetic disturbances in motion estimation to provide feedback to wearable robotic systems," *IEEE Trans. Neural Syst. Rehabil. Eng.*, vol. 25, no. 12, pp. 2398–2406, Dec. 2017.

[30] J. Favre, B. M. Jolles, R. Aissaoui, and K. Aminian, "Ambulatory measurement of 3D knee joint angle," *J. Biomech.*, vol. 41, no. 5, pp. 1029–1035, 2008.

[31] D. Roetenberg, H. J. Luinge, C. T. M. Baten, and P. H. Veltink, "Compensation of magnetic disturbances improves inertial and magnetic sensing of human body segment orientation," *IEEE Trans. Neural Syst. Rehabil. Eng.*, vol. 13, no. 3, pp. 395–405, Sep. 2005.

Matjaž Mihelj (M'10) received the B.Sc., M.Sc., and Ph.D. degrees in electrical engineering from the University of Ljubljana, Ljubljana, Slovenia, in 1996, 1999, and 2002, respectively.

Since 2014, he has been a Full Professor with the Faculty of Electrical Engineering, University of Ljubljana.

Janez Podobnik received the B.Sc. and Ph.D. degrees in electrical engineering from the University of Ljubljana, Ljubljana, Slovenia, in 2004 and 2009, respectively.

He is currently a Researcher with the University of Ljubljana. His current research interests include haptic interfaces, real-time control of robots for virtual-reality-supported rehabilitation, and sensory fusion techniques.

Marko Munih (M'88) received the Ph.D. degree in electrical engineering from the University of Ljubljana (UL), Ljubljana, Slovenia.

From 2004 to 2006, he was the Head of the Department for Measurements and Process Control, Faculty of Electrical Engineering, UL, where he is currently a Full Professor and the Head of the Laboratory of Robotics.